

Potential and scientific requirements of optical clock networks for validating satellite gravity missions

Stefan Schröder¹, Simon Stellmer², Jürgen Kusche¹

¹ *Institute of Geodesy and Geoinformation, University of Bonn*

² *Physics Institute, University of Bonn*

SUMMARY

The GRACE and GRACE-FO missions have provided an unprecedented quantification of large-scale changes in the water cycle. Equipped with ultraprecise intersatellite ranging links, these missions collect measurements that are processed further to monthly sets of spherical harmonic coefficients of the geopotential, which then can be converted into estimates of surface mass variation. However, it is still an open problem of how these data sets can be referenced to a ground truth.

Meanwhile, stationary optical clocks show fractional instabilities below 10^{-18} when averaged over an hour, and continue to be improved in terms of precision and accuracy, uptime, and transportability. The frequency of a clock is affected by the gravitational redshift, and thus depends on the local geopotential; a relative frequency change of 10^{-18} corresponds to a geoid height change of about 1 cm. Here we suggest that this effect could be further exploited for sensing large-scale temporal geopotential changes via a network of clocks distributed at the Earth's surface. In fact, several projects have already proposed to create an ensemble of optical clocks connected across Europe via optical fibre links.

Our hypothesis is that a clock network spread over Europe – for which the physical infrastructure is already partly in place – would enable us to determine temporal variations of the Earth's gravity field at time scales of days and beyond, and thus provide a new means for validating

satellite missions such as GRACE-FO or a future gravity mission. Mass changes at the surface of an elastic Earth are accompanied by load-induced height changes, and clocks are sensitive to non-loading (e.g. tectonic) height changes as well. As a result, local and global mass redistribution and local height changes will be entangled in clock readings, and we argue that very precise GNSS height measurements will be required to separate them.

Here, we show through simulations how ice (glacier mass imbalance), hydrology (water storage) and atmosphere (dry and wet air mass) variations over Europe could be observed with clock comparisons in a future network that, however, follows current design concepts in the metrology community. We assume different scenarios for clock and GNSS uncertainties and find that even under conservative assumptions – a clock error of 10^{-18} and vertical height control error of 1.4 mm for daily measurements – hydrological signals at the annual time scale and atmospheric signals down to the weekly time scale could be observed.

Key words: Time variable gravity – Europe – Time-series analysis.

1 INTRODUCTION

Launched in 2002, the Gravity Recovery and Climate Experiment (GRACE) has observed the time-variable gravity field of the Earth for over fifteen years. GRACE data have opened new avenues in fields such as the terrestrial water cycle, sea level rise, and glacier research (e.g. Tapley et al., 2019; WCRP Global Sea Level Budget Group, 2018). Since 2018, the GRACE data record is continued by the successor mission GRACE-FO (Flechtner et al., 2016), and several strategies for Next Generation Gravity Missions (NGGMs) have been proposed. Improved or new instruments like the GRACE-FO Laser Ranging Interferometer and different orbit configurations (e.g. Panet et al., 2013; Elsaka et al., 2014) promise to further improve the uncertainty and resolution of the gravity fields.

While the GRACE/-FO data are widely used now in environmental monitoring and starts to enter Earth system model simulations via data assimilation (Schumacher et al., 2016), it is still difficult to assess the 'true' errors of these data products. Thus, several techniques have been proposed for validation of GRACE data. Satellite Laser Ranging (SLR) has been used to derive

gravity field variations for a long time, but only low degrees can be utilized for validating GRACE spherical harmonic coefficients (Cheng & Ries, 2017). Using superconducting gravimeters (SG) for validating GRACE is under debate due to their sensitivity to local hydrological conditions and wet air masses (see van Camp et al., 2014 and Crossley et al., 2014). Also, several studies identified a clear common signal between GNSS derived height changes and GRACE (Davis et al., 2004; Chanard et al., 2018). However, tectonics, glacial isostatic rebound, aquifer compaction and groundwater recharge all affect GNSS measurements of deformation but do not follow elastic loading theory and cannot be derived from GRACE measurements only. This is critical in Europe in particular, where the loading signal is comparably low. In addition, it has been recently proposed to declare Terrestrial Water Storage (TWSA) an Essential Climate Variable (ECV), which will further underline the significance of monitoring TWSA, as well as providing validation for satellite data products.

Optical clocks (Ludlow et al., 2015) have seen a steady increase in performance over the past 30 years. Today's best clocks in leading metrology laboratories reach fractional instabilities at or below the 10^{-18} range, and are continuously improved in terms of stability and accuracy, dead-time free interrogation (Schioppo et al., 2017), transportability (Koller et al., 2017), and continuous realization of a timescale (Grebing et al., 2016). By comparing the tick-rates of two resting clocks, one can measure the difference in gravity potential acting on these clocks, due to the relativistic redshift effect. A frequency shift of one part in 10^{18} corresponds to about $0.1 \text{ m}^2 \text{ s}^{-2}$ potential difference, or 0.01 m geoid height difference. Clock comparisons over large spatial scales have been conducted in Europe between national metrology institutes *Système de Références Temps-Espace* (SYRTE) in Paris and *Physikalisch-Technische Bundesanstalt* (PTB) in Braunschweig (Lisdat et al., 2016). Further terrestrial links have been established between Paris and London as well as between Polish metrology laboratories. In the framework of the project *Clock Network Services* (CLONETS) it has been suggested to extend these existing links to a pan-European network (Krehlik et al., 2017).

Terrestrial fibre link technology has evolved over recent years, largely driven by communication needs. However, while all potential network sites considered in this study are already con-

nected to fibre networks, standard infrastructure and common network protocols do not allow for stabilities in the 10^{-16} range. Whether fibre networks can achieve stabilities required for optical clock comparison, depends on investment in tailored hardware: Turza et al. (2020) suggest that with duplex unidirectional signal transfer in existing (i.e. operational, soil-deployed) dense wavelength-division multiplexing (DWDM) telecommunication networks one can achieve 1-day averaging stability in the range 10^{-16} . Chiodo et al. (2015) built a coherent fibre link over more than 1000 km with uncertainties of 10^{-16} at 1 s integration time and 10^{-20} at 60.000 s integration time, via augmenting existing DWDM internet infrastructure by custom-made hardware in a few network nodes (their signal ran largely parallel with the internet data traffic). Using a dedicated fibre network employing cascaded Brillouin amplification finally, Raupach et al. (2015) demonstrated optical frequency transfer uncertainties at the 10^{-20} level and below.

Clock comparisons have been evaluated against measured height differences (Takano et al., 2016; Mehlstäubler et al., 2018), but here we go one step further, by suggesting that for validating mass change from GRACE-FO and NGGM's one would have to keep errors below the limits set by high-precision geophysical GNSS monitoring equipment. This means that errors in clock comparisons would have to be corresponding to the millimeter scale or 10^{-19} fractional frequency uncertainty. A network of clocks with a corresponding low noise floor would improve over monitoring mass-induced loading with geodetic GNSS networks alone because it would be sensitive to mass redistribution induced potential change as well as elastic loading, but it would also observe non-elastic (e.g. human-induced) and non-loading (e.g. tectonic) height changes. However, in combination with collocated permanent GNSS measurements for height control, the mass effect would be separable. We expect that this combination would be favourable compared to networks of terrestrial gravimeters because the gravity potential is less influenced by local mass changes than the gravity acceleration.

Voigt et al. (2016) provide an overview of the relevant tidal and non-tidal time-variable effects that are expected to alter clock rates. Leßmann & Müller (2018) analysed the effect of non-tidal ocean loading at hypothetical German and French clock locations, concluding that potential variations can reach amplitudes of up to $0.5 \text{ m}^2 \text{ s}^{-2}$ at coastal sites (5×10^{-17}). Along a different line of

reasoning, Lion et al. (2017) investigated the use of optical clocks in combination with measured gravity disturbances for regional geoid determination.

In this study, we propose to assess, via simulations, how non-tidal time-variable geophysical signals could be observed with a network of clocks, equipped with collocated, high-precision GNSS height control. We construct three noise scenarios, assuming white noise for the clock fractional frequency readings with standard deviations of 10^{-18} (10^{-19} , 10^{-20}) and a combination of flicker and white noise for GNSS with errors corresponding to a total noise variance of 1.4 (0.7, 0.3) mm. We neglect noise contributions stemming from the fibre link, as experimental studies have shown that this contributes less than 10^{-20} when dedicated fibre hardware is used (Raupach et al., 2015; Lisdat et al., 2016). We simulate time series of clock comparisons and subsequently analyse these in the time and frequency domain, which then enables us to identify which geophysical signals could be detected under which scenario. Despite the fact that geophysical mass change signals are low compared to other regions of the world, here we focus on Europe since infrastructure is already existing and the likelihood of establishing a clock network with the required noise floor in the coming decade is comparably high. We leave out tidal effects and non-tidal ocean mass and loading effects, and focus on atmosphere, hydrology, and glaciers.

This paper is structured as follows. In Section 2, we provide a background to chronometric geodesy and describe how we simulate noise of GRACE, clocks, and GNSS. Section 3 covers our simulated clock network and the signal simulation over Europe, which is then analysed in the spectral domain in Section 4. We discuss implications of our results in Section 5, and we discuss a few issues that will occur with the realization of a clock network. In Section 6 we summarize our conclusions.

2 BACKGROUND AND NOISE MODELLING

2.1 Background

Large-scale hydrological, climatic and geophysical processes are accompanied by mass redistribution at the Earth's surface, which in turn cause geopotential changes δV , gravity changes, and orbit perturbations of satellites. The GRACE and GRACE-FO missions measure these perturbations via inter-satellite ranging and precise orbit determination, and subsequent level 1 - 2 processing provides the geopotential with monthly resolution. It is this signal that we propose to be identified in clock comparisons here, and that can be represented through the dimensionless, fully normalized spherical harmonic coefficients (SHC) δv_{nm}

$$\delta V = \frac{GM}{a} \sum_n \left(\frac{a}{r}\right)^{n+1} \sum_m \delta v_{nm} \bar{Y}_{nm} \quad (1)$$

where δv_{nm} is a vector of the Stokes coefficients s_{nm} and c_{nm} , and the spherical harmonic functions \bar{Y}_{nm} contain the Legendre functions. GM is the geocentric gravitational constant, a the semimajor axis of the Earth taken as a reference radius, and r the radial distance to the geocenter. In what follows we will always consider mass changes at the surface of the Earth and thus identify r with a , but this does not limit the applicability of our proposed approach. Under the thin-shell assumption, Eq. (1) can be easily solved for the spherical harmonic coefficients of a surface mass distribution that generates δV . Taking further into account the elastic loading of the Earth's crust, the surface mass change field described by the SHC's $\delta\mu_{nm}$ is related as follows (e.g. Wahr et al., 1998):

$$\delta v_{nm} = \frac{1 + k'_n}{2n + 1} \delta\mu_{nm}. \quad (2)$$

The dimensionless load Love numbers k'_n characterize the response of the Earth's crust to the mass loading. With this the geopotential (δV), vertical surface displacement (δh) corresponding to elastic loading theory and the effective geopotential ($\delta V - g\delta h$) at the Earth's surface as defined in Voigt et al. (2016) would be, respectively:

$$\delta V = \frac{GM}{a} \sum_{n=0}^{\infty} \sum_{m=0}^n \frac{1 + k'_n}{2n + 1} \delta\mu_{nm} \bar{Y}_{nm}, \quad (3)$$

$$\delta h = \frac{GM}{a} \sum_{n=0}^{\infty} \sum_{m=0}^n \frac{h'_n}{2n+1} \delta \mu_{nm} \bar{Y}_{nm}, \quad (4)$$

$$\delta U = \delta V - g\delta h = \frac{GM}{a} \sum_{n=0}^{\infty} \sum_{m=0}^n \frac{1+k'_n-h'_n}{2n+1} \delta \mu_{nm} \bar{Y}_{nm}, \quad (5)$$

Equation (4) introduces the load Love numbers h'_n , denoting the elastic response of the Earth in terms of vertical surface displacement. For later use, we mention that the h'_n should correspond to k'_n in the sense that both are derived from the same 1D Earth model. Equation (5) is what a clock, sitting on the deforming crust, would measure (where we have set $g = -\frac{GM}{a^2}$).

For a single clock resting on the Earth's surface, temporal changes of the effective potential U would lead to temporal changes in fractional frequency due to gravitational redshift (e.g. Ludlow et al., 2015):

$$\frac{\delta f}{f} = \frac{\delta U}{c^2}, \quad (6)$$

where f is the atomic resonance frequency, δf is the change in the clock's frequency, and c equals the speed of light. For two clocks resting at different locations with geopotential U_1 and U_2 we have a difference

$$\frac{\Delta f}{f} = \frac{\Delta U}{c^2} = \frac{U_2 - U_1}{c^2}. \quad (7)$$

In the following we will look at the temporal changes of the effective potential δU that will occur for a terrestrial clock due to geodynamic and environmental/climate effects. We are interested in the sub-mm to cm level in terms of the geoid, which translates into 10^{-3} to 10^{-1} $\text{m}^2 \text{s}^{-2}$ of geopotential and into 10^{-20} to 10^{-18} fractional frequency. We assume that such uncertainty could be reached through averaging clock readings over periods of several minutes to a day. A comparison, when implemented over longer time and with a certain temporal resolution (i.e. a finite averaging interval) would then enable one to determine the time-variable contribution in ΔU :

$$\delta U_2 - \delta U_1 = \frac{(\delta f_2 + \varepsilon_{\delta f_2}) - (\delta f_1 + \varepsilon_{\delta f_1})}{f} \cdot c^2 \quad (8)$$

with the two clocks' respective errors $\varepsilon_{\delta f}$. In order to retrieve the time series of differential geopotential δV at a fixed reference height instead of differential effective geopotential δU , one would

need to correct for the vertical uplift δh :

$$\delta V_2 - \delta V_1 = (\delta U_2 + g\delta h_2) - (\delta U_1 + g\delta h_1) \quad (9)$$

$$= \left(\frac{\delta f_2 + \varepsilon_{\delta f_2}}{f} \cdot c^2 + g(\delta h_2 + \varepsilon_{\delta h_2}) \right) - \left(\frac{\delta f_1 + \varepsilon_{\delta f_1}}{f} \cdot c^2 + g(\delta h_1 + \varepsilon_{\delta h_1}) \right), \quad (10)$$

where we would have to account for errors in height corrections $\varepsilon_{\delta h}$.

2.2 GRACE/-FO noise

Due to the missions' orbital pattern and the anisotropic sensitivity of the inter-satellite leader-follower configuration, spherical harmonic coefficients from GRACE/-FO typically at monthly resolution are corrupted by anisotropic, latitude- and degree-dependent, and temporally non-stationary noise. This noise is induced by a combination of instrument errors, temporal aliasing of insufficiently corrected short-term mass signals, and orbit errors. Even nearly two decades after the GRACE launch, it is still difficult to realistically characterize errors for level-2 products, i.e. harmonic coefficients. This is mainly since no other measurement technique is able to determine geoid height variations with superior accuracy at large spatial scales. In lieu, comparing level-2 data from different processing centers has been suggested, but since processing strategies and background models are similar this cannot be expected to provide a realistic error level. Fitting simple models of trend and annual/semi-annual signal to GRACE data and estimating data errors from such fits has been suggested, but we know from geophysical modelling that real mass signals are rich in episodic and interannual variability which renders this approach overly conservative. Instead of a (still missing) community-agreed GRACE error model, we here use formal errors from Mayer-Gürr et al. (2018). We propagate these formal errors to geoid height errors at two assumed clock locations, in order to derive geopotential error variances and covariances at these locations. Consecutively, the (co-)variances are propagated to the variance of geoid height difference between the locations – this procedure enables us to take into account the effect of geographical latitude due to GRACE orbit convergence as well as the distance between clock locations, since larger-scale-errors tend to cancel out for differences at shorter distances.

GRACE-FO errors have been estimated as somewhat lower than for GRACE, due to the more

precise laser ranging instrument (Flechtner et al., 2016). For future gravity missions, simulation studies have predicted errors as low as ten to twenty times below GRACE-FO noise depending on orbit configuration, number of satellites and instrument types, but this will be likely limited by errors inherent to the short-time background geophysical models. In summary, we assume that future missions will surpass GRACE-FO, but that methods for assessing their errors will be dearly required.

2.3 Clock network noise

Clock comparisons yield effective potential differences ΔU , possibly at daily resolution (e.g. Chou et al., 2010; Ludlow et al., 2015). A clock’s uncertainty is usually characterized by an error resulting from systematic uncertainties and an error originating in the instability, expressed through its Allan deviation (Riley & Howe, 2008). By definition, any error related to the instability averages out with longer measurement time. For many state-of-the-art optical clocks the instability averages down below the systematic uncertainty within several minutes to hours (Bothwell et al., 2019; Oelker et al., 2019), albeit with our application of daily, relative measurements in mind, we are not interested in the systematic errors. What limits the noise floor here are effects like black body radiation or dc Stark shift, which need to be monitored permanently and for every clock individually (Ludlow et al., 2015; Bothwell et al., 2019). Because the properties of the errors stemming from this monitoring are not well investigated, we deem it sufficient here to simulate errors as white noise.

To account for technological progress, we will adopt three different scenarios for clock uncertainties, see Table 1. In scenario 1, here we work with a noise floor of 10^{-18} , which is what current state-of-the-art clocks are just reaching now (Bothwell et al., 2019; Oelker et al., 2019); even contemporary transportable clocks approach this order of magnitude (Takamoto et al., 2020). In scenario 2 we assume that clock noise can be decimated by one order of magnitude (10^{-19}) and this is what we expect clocks to reach in five to ten years. Scenario 3, in which we assume noise again decreased by one magnitude, i.e. 10^{-20} , is a ”best case” scenario for the clock network. It should be mentioned that these error assumptions refer to single clocks. The error of a clock com-

Table 1. Clock network and colocated GNSS error scenarios.

Error type	Scenario 1	Scenario 2	Scenario 3
Clock white noise	10^{-18}	10^{-19}	10^{-20}
GNSS white noise	1 mm	0.5 mm	0.2 mm
GNSS flicker noise	$4.4 \text{ mm/yr}^{0.25}$	$3.1 \text{ mm/yr}^{0.25}$	$2.0 \text{ mm/yr}^{0.25}$

parison originates from the noise of the two clocks and the error that the fibre link adds; we will thus assume 1.4×10^{-18} (10^{-19} , 10^{-20}) uncertainty for a clock comparison. Experimental studies have shown that the fibre link itself contributes less than 10^{-20} to the clock comparison (Raupach et al., 2015), and we thus neglect noise contributions from the fibre link in our studies, independent of the distance.

As has been suggested in the above, in order to separate the potential δV from the effective potential δU we need to correct for $g\delta h$ (Eq. 10). It is obvious that errors in δh fully translate into geoid height error; 1 mm height or geoid height error corresponds to 1.1×10^{-19} fractional frequency error. In line with the GNSS literature (Williams et al., 2004; Klos et al., 2017), we assume that vertical displacement time series derived from GNSS are affected by both white noise and flicker noise, where the latter can be identified with power-law noise with spectral index $\kappa = -1$. White noise in GNSS errors results e.g. from phase errors or unmodelled short term propagation effects, flicker noise from tide model or orbit constellation errors (Agnew & Larson, 2007). In the noise model that we construct here, we assume that both white noise and flicker noise contribute evenly to the total variance in the daily measurements we simulate. The values for the GNSS flicker noise in Table 1 are computed after Bos et al. (2013). Orientating towards Klos et al. (2016) and Gruszczynska et al. (2018) we assume that white noise and flicker noise add each about 1 mm^2 noise variance, resulting in an assumed overall height error Root Mean Square (RMS) of 1.4 mm. This corresponds to assuming that each clock is accompanied by an IGS-type (International GNSS Service, Villiger & Dach, 2020) GNSS antenna and that time-variable height differences between clock and local antenna can be controlled with superior accuracy, e.g. by repeated levelling.

Under scenario 2 and 3 we assume that both white noise and flicker noise will be reduced. We hypothesize that under scenario 2, i.e. within five to ten years, noise in troposphere and GNSS

orbit and clock errors etc. can be further reduced, e.g. through rapid development of multi-GNSS analyses. Under scenario 3, we assume that errors can be – as for the clock rate uncertainties – further reduced to a level of 0.3 mm, which would likely require next-generation GNSS systems (Giorgi et al., 2019; Glaser et al., 2020). The assumed reduction of uncertainty between the scenarios is larger for the clocks than for GNSS, which is probably realistic considering the evolution in clock techniques over the last decades (Poli et al., 2013), while GNSS for height control will be always limited by errors in tropospheric and ionospheric modelling. In addition, GNSS could in future benefit from common-clock linking to the National Metrology Institutes’ optical clock time reference.

At this point we notice that the typical RMS fits from GRACE-derived vertical deformation or from geophysical load models evaluated versus time series of GNSS height measurements can still be a few millimeters (Chanard et al., 2018) – as these comparisons employ elastic loading theory and detrending, these fits must inevitably include residual vertical motion signals as well as troposphere errors and site-specific effects. As a result, such comparisons cannot serve for developing a GNSS error model.

We expect that for comparing monthly geopotential change derived from GRACE/-FO or from future gravity missions and the daily, relative fractional frequency changes within a clock network, one would convert the fractional frequency changes to geoid height changes and average these to monthly data. We do not expect that the clock network errors will average out following a white noise behaviour, i.e. decrease with averaging time. Rather we expect that certain error contributions will be reduced, like errors in tide models, whereas others such as clock drift may increase. In the absence of a better knowledge of the individual error sources, we will assume here that monthly averages of relative clock rates will not further improve over daily rates. For the computation of monthly GNSS error estimates we take temporal correlations into account by using the Power Spectral Density (PSD) of the power-law noise that we constructed; the integral over the PSD, starting at monthly frequencies, equals the variance of monthly errors.

Table 2. Stations assumed here to participate in a clock comparison network. The national metrology institutes are written in bold.

Location	Institution	Abbr.	Country	Lon/Lat [°]
Vienna	Federal Office of Metrology and Surveying	BEV	Austria	16.4/48.2
Prague	CESNET Association of legal entities	CESNET	Czech Republic	14.5/50.1
Helsinki	National Metrology Institute of Finland	MIKES	Finland	24.8/60.2
Paris	Time Space Reference Systems, Paris Observatory	SYRTE	France	2.2/48.8
Strasbourg	University of Strasbourg	US	France	7.8/48.6
Braunschweig	Physikalisch-Technische Bundesanstalt	PTB	Germany	10.4/52.3
Bonn	University of Bonn	UB	Germany	7.1/50.7
Munich	Max Planck Institute of Quantum Optics	MPG	Germany	11.5/48.2
Potsdam	GeoForschungsZentrum	GFZ	Germany	13.1/52.4
Wetzell	Geodetic Observatory	GOW	Germany	12.9/49.1
Torino	Italian National Metrology Institute	INRiM	Italy	7.6/45.0
Delft	Dutch Metrology Institute	VSL	Netherlands	4.4/52.0
Poznan	Supercomputing and Networking Center	PSNC	Poland	17.0/52.4
Torun	University of Torun	UT	Poland	18.6/53.0
Warsaw	Central Office of Measures	GUM	Poland	21.0/52.2
Ljubljana	Slovenian Institute of Quality and Metrology	SIQ	Slovenia	14.5/46.0
Gothenburg	National Laboratory for Length and Dimensional Metrology, Research Institutes of Sweden	RISE	Sweden	12.0/57.7
Bern	Federal Institute of Metrology	METAS	Switzerland	7.4/46.9
London	National Physical Laboratory	NPL	United Kingdom	0.3/51.4

3 SIMULATION SETUP

3.1 Network

For our simulation we assume that most of Europe’s national metrology institutes and other UTC-laboratories will be equipped with ultra-precise clocks, and that fibre links exist already or will be successively established between them. The geographical distribution of the institutes are visualized in Fig. 1 and are as in Table 2. Moreover, we took the liberty to add a few additional sites (Wetzell, Potsdam, Bonn) for potential deployment of precise clocks and expansion of the fibre network, which are under consideration for additional metrological experiments in the geodetic



Figure 1. Assumed network geometry. Red fibre links with dedicated hardware for ultra-precise clock comparisons are already existing, blue dashed links are additional connections that we consider here.

context. With this setup we take the following assumptions: 1) One optical clock is located at every site marked in Fig. 1. 2) At every clock, an IGS-type GNSS-site is colocated in order to correct for land elevation change. 3) One would be able to carry out measurements of relative fractional frequency differences between all the clocks during a single session every day, which have an integration time sufficiently long for the instability to drop below the systematic uncertainty.

The outcome of this configuration would be one daily geopotential time series per clock relative to a chosen reference clock. In other words, we assume that one of the clocks would serve as a reference clock for all others. We are aware that other concepts could be devised, e.g. defining a reference frequency standard via averaging all clocks, but this would not change our experiment significantly. In either case, as in GNSS network analyses, large-scale, common-mode geopotential and height change signals that affect all clocks in the same way could not be detected. This is,

however, an imperative consequence of the clock comparison method, unless we can anchor clock comparisons via free-space links to a reference clock in space (Mehlstäubler et al., 2018). In what follows, we explore to what extent such a setup would enable one to detect spatiotemporal changes of the gravity field over Europe, and thus could provide a reference for gravity missions. We do not discuss the objective of realizing a unified height reference system here (Lisdat et al., 2016).

Then, in an additional experiment we extend this setup by assuming that all the EUREF permanent network GNSS stations would be accompanied by clock measurements. The purpose of this scenario is to understand how beneficial a denser clock network could be for monitoring gravity change and mass redistribution at a spatial scale down to tens of kilometers.

3.2 Simulated signal

For a single location, we can write the effective potential as

$$U = \bar{U} + \delta U^T + \delta U^{NT} - g\delta h \quad (11)$$

with time-mean \bar{U} , tidal variations δU^T and nontidal variations δU^{NT} . As mentioned before, any vertical motion of the surface δh will also translate into a potential change at that surface. Usually, tidal potential variations are split into direct astronomical (tide-generating) potential δU^{TGP} , Earth tide potential δU^{ET} , ocean tides δU^{OT} , and atmospheric tides δU^{AT} . The nontidal potential variation contains contributions from mass redistributions in the atmosphere δU^A , ocean δU^O , cryosphere δU^I , and the solid Earth δU^S , and from Glacial Isostatic Adjustment δU^{GIA} and hydrology δU^H , i.e. surface and groundwater storage changes.

Here, we focus on the nontidal part of the potential induced by atmospheric mass variations δU^A and by storages changes in hydrology δU^H . We simulate atmospheric mass variability following Forootan et al. (2013) with with 3D pressure and moisture data from ERA5 (Copernicus Climate Change Service (C3S), 2017). δU^H is derived from water storage in thirty layers simulated with the Community Land Model (CLM; Oleson et al., 2003) 3.5, forced by the Weather Research and Forecasting (WRF; Skamarock et al., 2008) version V3.3.1. As a result, for these two contributions we obtain daily values of total water storage anomalies. δU^H and δU^A are sim-

ulated over the year 2007. Mass redistributions due to retreat or thickening of glaciers in the Alps and Scandinavian mountains is simulated with the Open Global Glacier Model (OGGM, Maussion et al. 2019), which is forced by CRU TS4.01 (Harris et al., 2014) data. The temporal resolution of the OGGM output is limited to monthly values, but we construct a longer time series from October 2005 to September 2008. We represent the corresponding potential via spherical harmonic coefficients of maximum degree 720 for δU^H and δU^I , and degree 180 for δU^A , which corresponds to a half-wavelength of 111 km and 28 km, respectively.

For hydrological, atmospheric, and glacier mass changes, the variability with respect to the 2007 mean (Fig. 2, columns one, two, and three, respectively) reaches up to 40 (15, 40) cm when expressed in equivalent water height (EWH, first row), and 2 (6, 0.5) mm in corresponding geoid changes, visualized in the last row. The hydrological signal shows high variability in the mountain regions of Scandinavia and in the Alps. Since the signal over Europe contains much energy at smaller spatial scales, the effect on the geoid is rather small. This is very different from other regions of the world, such as the Amazon, where geoid variability reaches 1-2 cm. After removing a six-parameter model that contains linear trend, annual and semiannual signals, the variability drops to 15 cm EWH; this is shown in the second row of the figure, without corresponding geoid height. To focus on the sub-monthly signal, we have additionally applied a thirty-day boxcar filter. This results again in a distinct decrease in variability, reaching about one order of magnitude in the mountain regions compared to the full signal. We note that the day-to-day variability is in particular interesting since neither GRACE/-FO nor future gravity missions are likely able to monitor this signal at an appropriate spatial resolution.

For the atmosphere (second column) we see a much smoother picture of EWH variability. This partly stems from the fact that the maximum spherical harmonic degree of our simulated atmospheric potential coefficients is only 180, corresponding to a spatial resolution of 110km. This is governed by the ERA5 spatial resolution, and experiments with high-resolution regional models (Dobslaw et al., 2016) suggest that atmospheric mass variability at higher degrees is predominantly driven by topographic variability and in general low. The main reason for the smoothness though is probably the large size of atmospheric high and low pressure areas. Here, we do not

see large differences after removal of long-term signals; in fact the variability is concentrated at higher temporal scales, it is between 11 and 13 cm EWH. This illustrates the low seasonality of the atmospheric mass. For Europe, with up to 5mm geoid height RMS the large scale atmospheric variability transfers to a higher geoid height variability as compared to hydrological storage changes.

The last column shows the RMS variability resulting from glacier simulations in the Alps and the Scandinavian mountains. This shows a picture very similar to that of the hydrology, but somewhat more localized because the variations are limited to glaciated areas. Our hydrological model contains a snow component; it is thus expected that patterns are similar. One might argue that these two models thus simulate similar processes in mountainous regions. However, since the glacier model contains a much more sophisticated representation of ice storage and thus provides a more realistic picture, we have decided to work with all three models. In our analyses we do not interpret the combination of the models in the sense of the sum of effect, though.

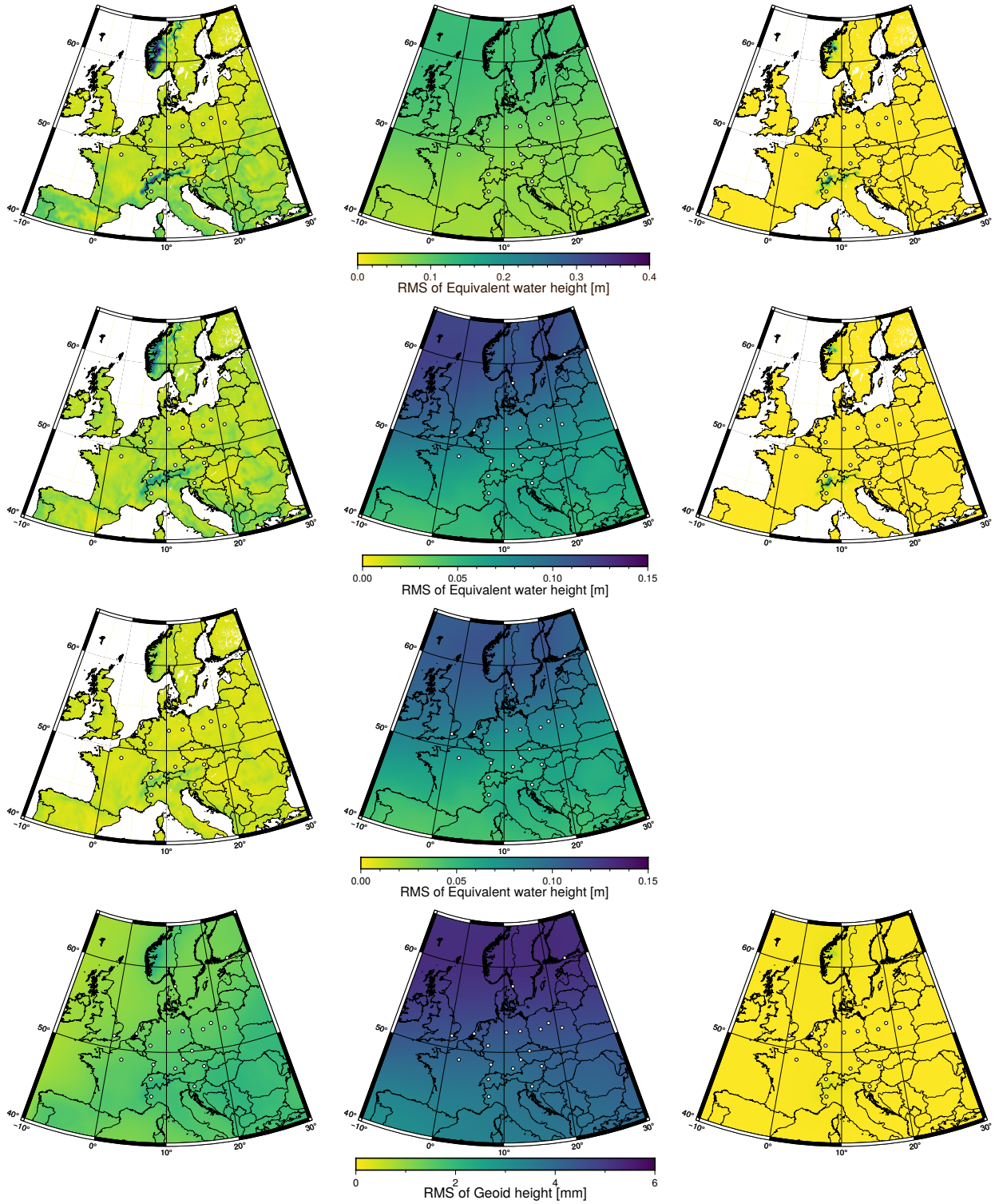


Figure 2. 2007 equivalent water height root mean square (RMS) variability of daily hydrologic (first column) and atmospheric (second column) mass redistribution signal expressed in equivalent water height, as well as monthly glacial (third column) signal from 2005 to 2008. The first row shows the full signal, the second row shows the RMS after de-trending and de-seasoning, and in the third row the day-to-day signal variability only is shown. The last row shows resulting geoid height RMS of the full signal, thus corresponding to the first row.

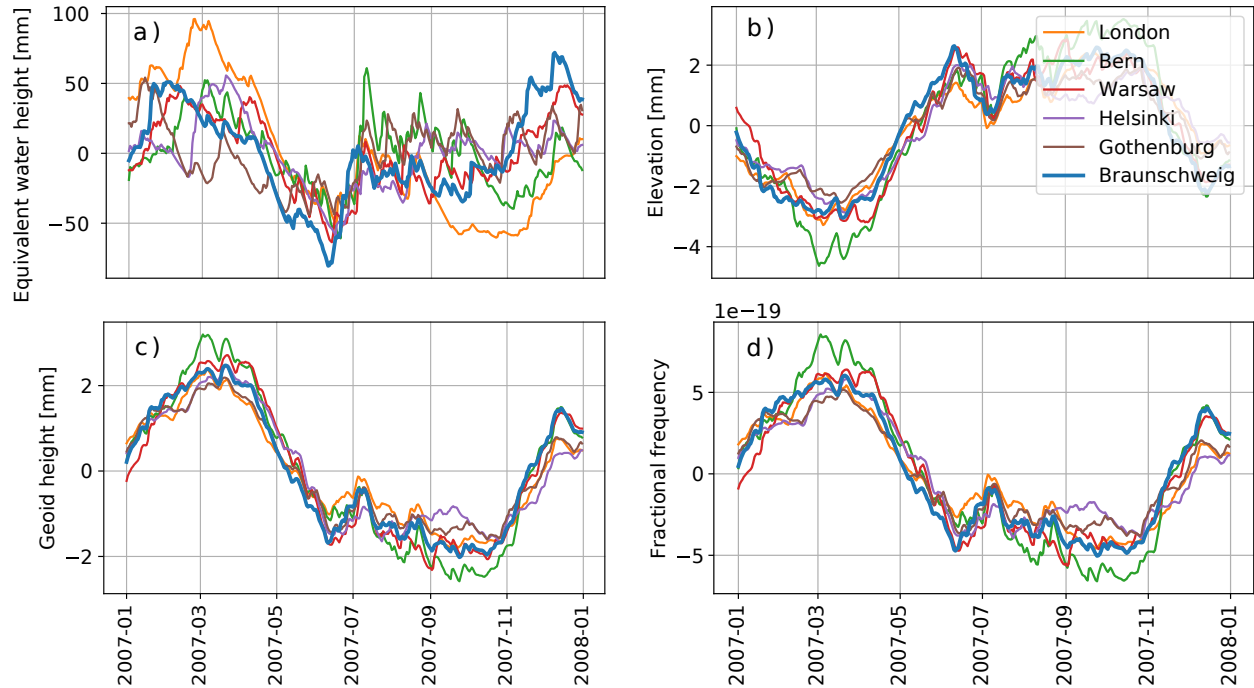


Figure 3. a) Daily hydrological storage variations at several stations in 2007 and resulting b) elevation, c) geoid height, and d) fractional frequency variations.

4 RESULTS

In this section, we analyse time series of simulated fractional frequency variation for individual clock locations, which were simulated using models for atmospheric, hydrological, or cryospheric mass variability over Europe, as explained in Section 3. We are showing exemplary time series for clocks in Braunschweig, London, Bern, Warsaw, Helsinki, and Gothenburg, whose geographical locations are well spread over the network area. Our focus will be on surface mass changes, the resulting vertical displacement, geoid (potential) change, and in particular the fractional frequency change.

4.1 Hydrological storage changes

Comparing the the time series corresponding to hydrologic storage changes in 2007 (Fig. 3), the annual signal can be seen in every time series. However, surface mass changes expressed in equivalent water height (EWH, a) differ significantly from clock to clock. This is due to the influence of regional/local hydrology, which is here included up to the 10km scale via the CLM model, i.e. omitting only very local effects. However, such regional-to-local scale mass changes will affect

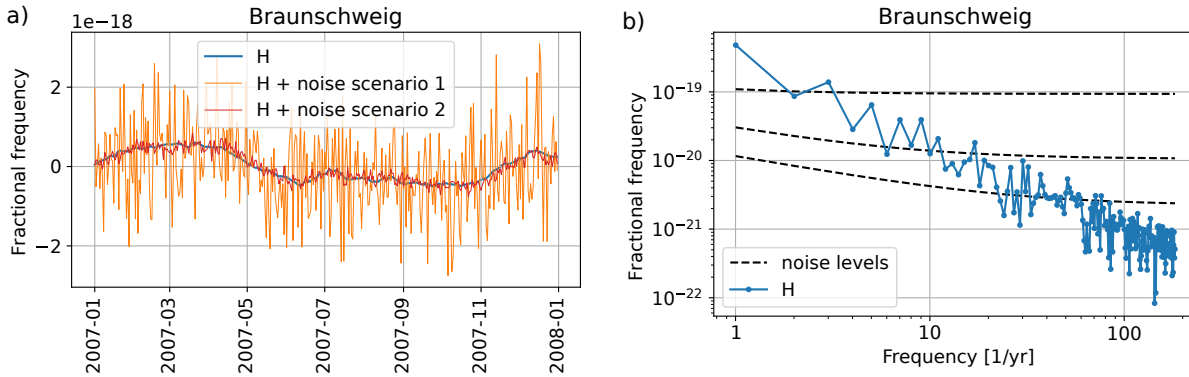


Figure 4. a) Comparison time series of hydrology-induced (“H”) fractional frequency changes for **Braunschweig** and b) in the spectral domain.

vertical displacement (b) and geoid height change (c) much less than effects of larger spatial scale, thus these two signals are very similar, albeit they show an opposing sign. Simulated displacement and geoid height change for the Bern site exhibit a slightly higher amplitude than at the other stations due to their proximity to the hydrologically highly variable Alps. The fractional frequency (d) variations result directly from the geoid height and the vertical displacement. Although elastic loading theory predicts that land elevates when geoid heights decrease due to surface mass redistribution, they both will contribute to geopotential changes with the same sign, and this will then lead to an amplified fractional frequency change. It is this fractional frequency change and its magnitude, which is of key interest here. We observe an amplitude of circa 10^{-18} , thus in the cm-range of physical heights.

Exemplarily for Braunschweig, the time series is shown with added noise from scenarios 1 (10^{-18} clock error and 1.4 mm GNSS error) and 2 (10^{-19} and 0.7 mm) in Fig. 4a). The scenario 3 noise (10^{-20} and 0.4 mm) is left out since it is too small to be distinguishable. The noise levels are also shown in relation to the corresponding amplitude spectrum (4b), where it can be observed that the annual signal is well above the scenario 1 noise level, but to shorter-term signals would not stick out of the noise in this case. In contrast, for scenario 2, frequencies beyond a month would be detectable against the noise floor. We conclude that for identifying signals at even higher frequencies, a lower clock and/or GNSS uncertainty would be needed.

In order to observe changes in clock tick rates, one would need to perform clock comparisons. The simulated clock comparison time series and its corresponding amplitude spectrum between

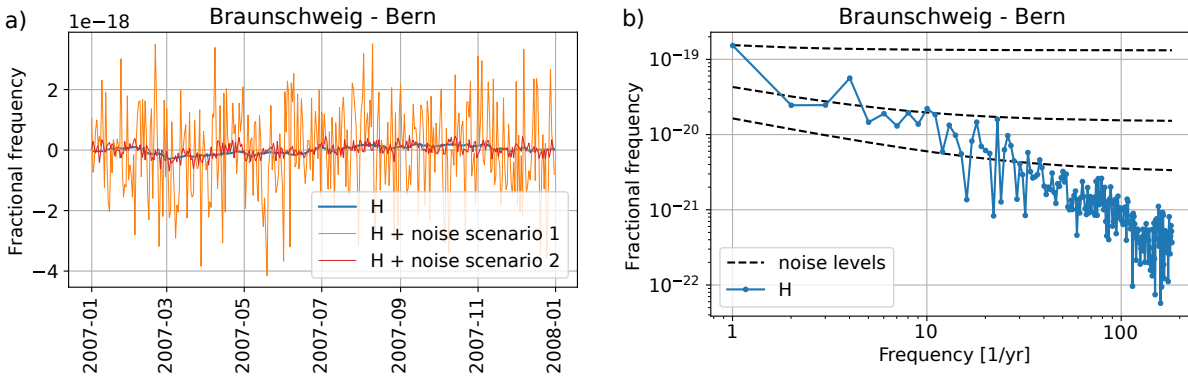


Figure 5. a) Comparison time series of hydrology-induced fractional frequency changes for the link **Bern vs. Braunschweig** and b) the amplitude spectrum of it.

PTB (Braunschweig) and METAS (Bern) can be seen in Fig. 5. As expected, the observable relative fractional frequency change would be smaller than for a single clock, because the distance of the two locations is only 630km, thus low degree signals affect both clocks to a similar extent and cancel out. The annual signal is thus reduced from 5×10^{-19} to 1.5×10^{-19} and would just reach the noise level of scenario 1, which at the same time is slightly elevated due to the differencing approach. For the higher frequencies, almost no single frequency amplitude would stick out of the noise level of scenario 2, and only signals up to a biweekly frequency are above the assumed noise of scenario 3. This is an important outcome of this analysis, since it suggests that short-term hydrologic mass changes would not significantly affect clock comparisons.

In order to review this statement drawn from a single link, we show time series and amplitude spectra of several stations compared to Braunschweig in Fig. 6. Although the time series differ

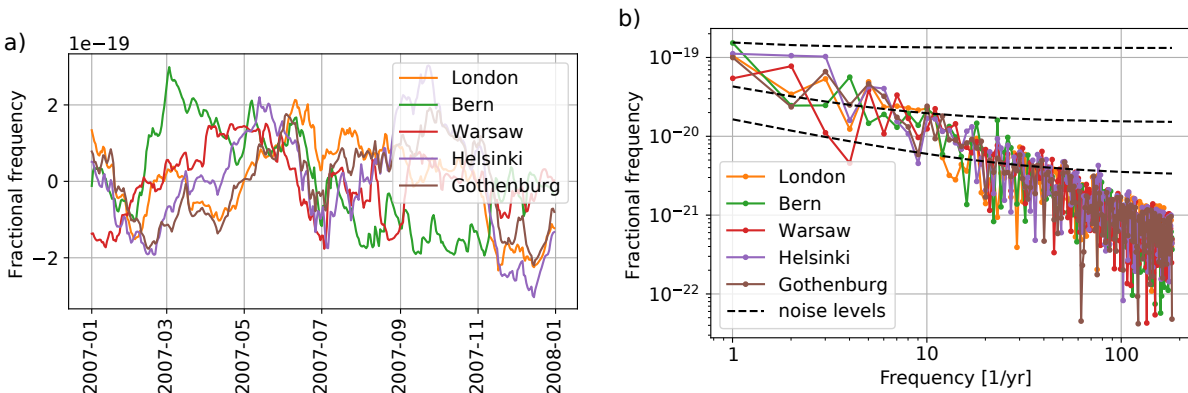


Figure 6. a) Fractional frequency variations induced by hydrological mass redistribution relative to **Braunschweig**. b) Corresponding amplitude spectrum including the three noise levels for clock comparisons.

substantially – now that a large part of the common annual signal is removed within the differencing approach – their spectra all resemble closely the one predicted for the simulated link Bern vs. Braunschweig analysed before.

Although individual peaks are almost all below 10^{-19} , one will notice that after integration the signal level amounts to about 5×10^{-19} . For comparison, Voigt et al. (2016) report ranges of 10^{-18} over Europe in 2003-2004 (they used spherical harmonic coefficients up to degree and order 100 based on the GLDAS model), which is in alignment with what we show in Figure 3. For differences at clock locations over continental scales they report 10^{-18} as well, which is twice of what we find (compare Fig. 6). This may be related to a slightly different simulation setup; our study assumed a network which does not cover the entire continent, and due to the differencing approach this will inevitably lead to some limitation in the maximum signal level. Generally, one can conclude from the fractional frequency simulations that short term hydrology, i.e. water storage changes at time scales below one month, can be neglected even for clock comparisons in scenario 2. In other words, given noise levels under scenario 2, they would not be detectable with such uncertainties of the clocks and GNSS. This conclusion would have to be revisited if one would bring a clock closer to a location in the Alps or the Scandinavian mountains though.

4.2 Atmospheric mass changes

In this section we will analyse the effect of atmospheric mass variability, which is both due to the redistribution of dry air masses and the corresponding pressure changes, and due to much faster water vapour variability. As the atmospheric mass variability is known to contribute much more to observed signals as compared to hydrological variability, Fig. 7 reveals a much larger amplitude of EWH variation, with 0.7 m about three to four times as high as the EWH amplitude induced by hydrological mass changes. This transfers to vertical displacement, geoid height, and fractional frequency as well. For our simulated network, we observe that maximum fractional frequency amplitudes lie in the range of 6×10^{-18} . Furthermore, there is no obvious annual signal observable, while the short term variations appear very high.

In Fig. 8 we show the simulated time series at the single clock location of PTB, Braunschweig

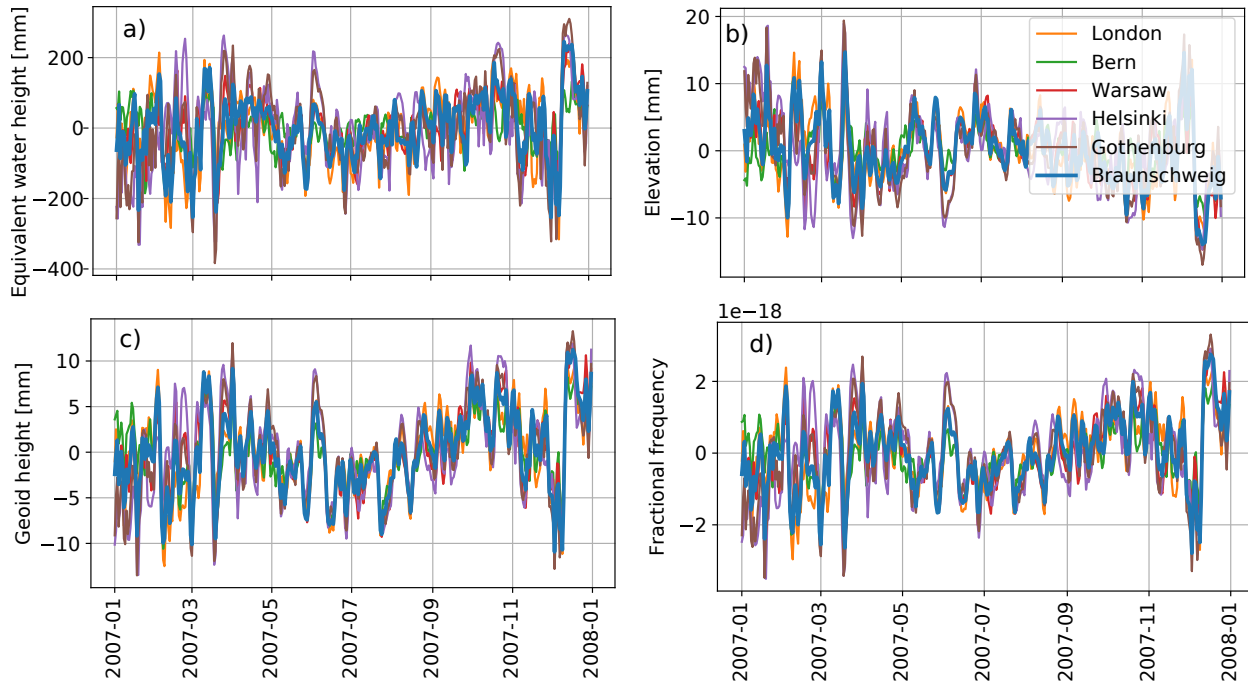


Figure 7. a) Daily atmospheric mass variations at several stations in 2007 and resulting b) elevation, c) geoid height, and d) fractional frequency variations.

again. The noise in scenario 1 is not as dominant as it appears compared to the hydrological signal, because the signal-to-noise ratio is higher. Also, up to a frequency of circa 30 cpa (cycles per annum) most of the signal spectrum appears well above the noise level for all three scenarios. When observing the simulated clock comparison times series and amplitude spectrum between Braunschweig and Bern (Fig. 9), one notices that in particular, the low frequency signal is reduced

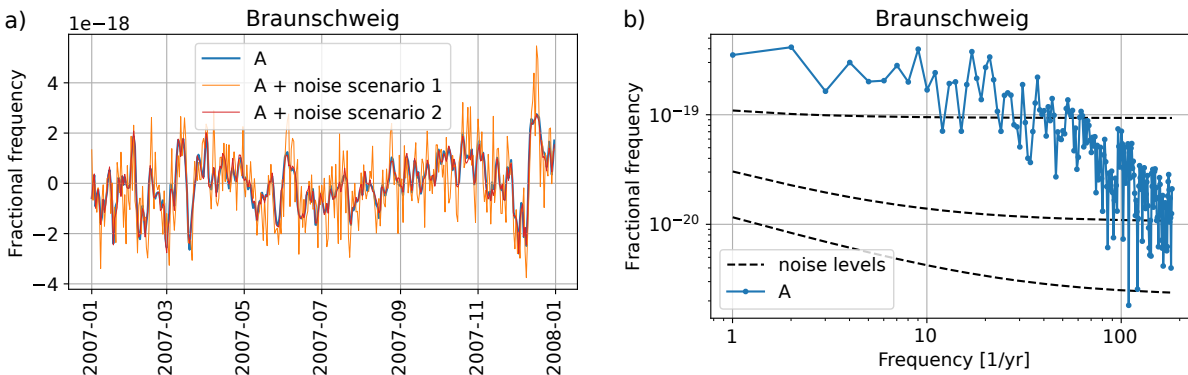


Figure 8. a) Time series of atmospheric mass induced fractional frequency variations in **Braunschweig** and b) the spectral domain of it.

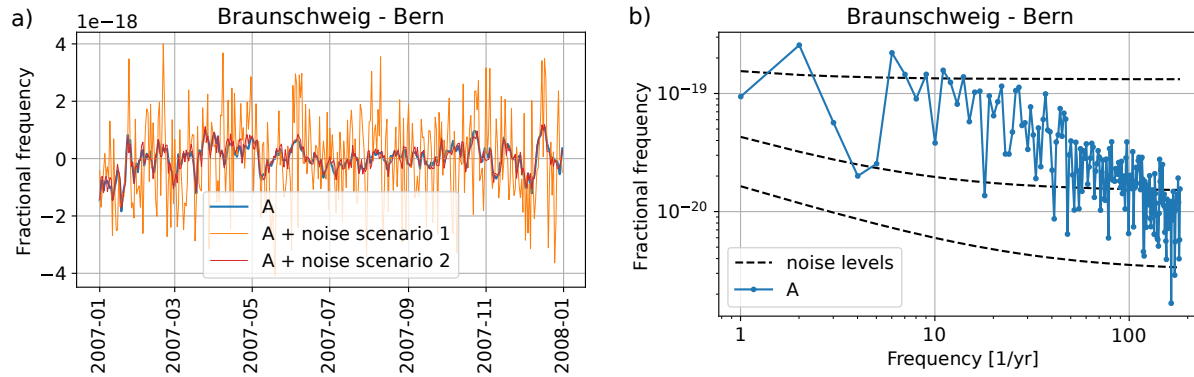


Figure 9. a) Comparison time series of atmospheric mass induced fractional frequency changes for the link **Bern vs. Braunschweig** and b) the spectral domain of it.

as compared to the single clock signal. Still, up to about 100 cpa the signal exceeds the noise floor of scenario 2.

When comparing simulated fractional frequency differences for the link Bern vs. Braunschweig to differences for the other links (Fig. 10), the connection between MIKES (Helsinki) and Braunschweig stands out. With 1250km distance, Helsinki is the location furthest away from Braunschweig. This highlights the influence of distance between the clocks, something that we did not observe to this extent for the hydrological effect. For a clock comparison along the link Helsinki vs. Braunschweig, one would find fractional frequency variations of up to 5×10^{-18} , thus almost as large as the single clock variations. Voigt et al. (2016) suggest geoid height and vertical displacement values during a storm surge in the North Sea which would add up to 2.5×10^{-18} relative to a mean value. This is similar to what we find (3×10^{-18} deviation from the mean, e.g. during a

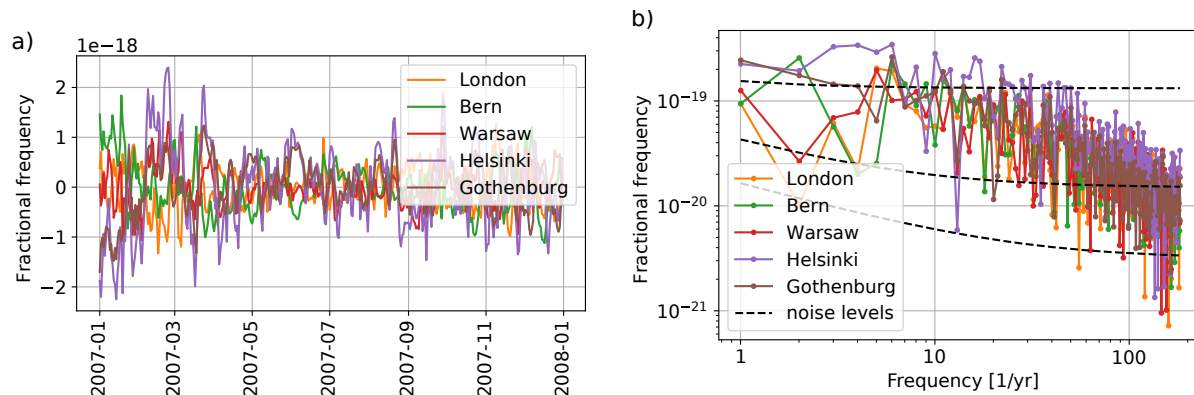


Figure 10. a) Atmospheric mass induced fractional frequency variations relative to **Braunschweig**. b) Corresponding spectral domain including the three noise levels for clock comparisons.

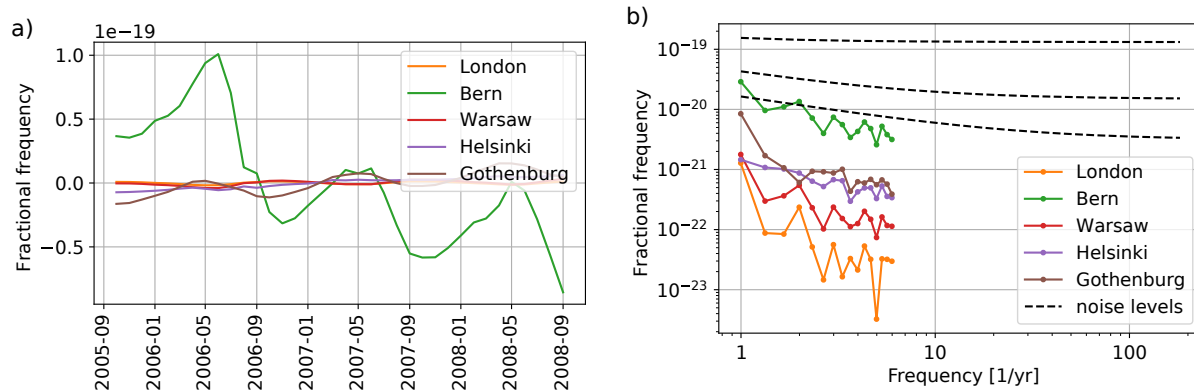


Figure 11. a) Glacier induced fractional frequency variations relative to **Braunschweig**. b) Corresponding amplitude spectrum including the three noise levels for clock comparisons.

deep depression leading to cyclone Kyrill in mid of January 2007). However, we mention in passing that, unlike noted in Voigt et al. (2016), the direction of the geoid change does not depend on whether the mass change is happening below the clock, i.e. groundwater and ocean mass change, or above the clock, i.e. glacial and atmospheric mass change. This can be conceptualized through imagining a 'mass disk' below, at, or above the Earth's surface: This mass disk leads to a jump in the gravity acceleration, with positive sign above, and negative sign below itself. Since the potential is the integral over the gravity acceleration along the vertical (Hofmann-Wellenhop & Moritz, 2005), it only leads to a cusp for the potential, with positive sign everywhere and maximum in itself. Interestingly, the clock comparisons over the network distances do not show much smaller variations than the single clock time series. This clearly points out the importance of atmospheric mass correction data for European fibre link optical clock comparisons at the spatial and temporal scales that we consider here, and that would be relevant for validating a future gravity mission.

4.3 Glacier mass variability

Glacier models are typically run at monthly resolution, due to the slow response behaviour of the glaciers. As a result, we analyse monthly glacier mass changes here, dating from October 2005 to September 2008. Although the time series is very short for an analysis in the spectral domain, some results are obvious: In Figure 11a) the simulated clock link from Braunschweig to Bern displays the highest fractional frequency variability with a distinct annual amplitude up to 1.3×10^{-19} . Gothenburg shows an annual signal as well but to a much smaller extent. That is observable in

the spectral domain as well, where Bern is the only location with single amplitudes exceeding the noise level of scenario 3. In conclusion, as long as the clock locations are not closer to glaciated areas than Bern is, the time variable signal of the glaciers will play only a minor role compared to hydrology and atmosphere induced mass redistributions. This will be true in the case of daily variations as well, as glacier changes are dominated by seasonal signal. What could become a factor, however, are long term trends, as glaciers undergo strong melting during global warming. Moreover, the total mass imbalance for European glaciers is estimated to only about 2 Gt yr^{-1} , compared to 73 Gt yr^{-1} for Alaskan glaciers (Zemp et al., 2019) or to the mass imbalance of the Greenland ice sheet, quantified to -272 Gt yr^{-1} by the WCRP Global Sea Level Budget Group (2018).

5 DISCUSSION

Time-differencing clock comparisons measure differences in geopotential change with differential height changes superimposed. At the time being, using colocated, high-precision GNSS measurements appear the best choice for separating the geopotential. As we have shown, the GNSS uncertainty will soon become a limiting factor for clock comparisons on the ground. This requires additional discussions; we will focus on two potential remedies here:

A straightforward option could be instead of relying on GNSS to co-estimate the elastic loading jointly with the geoid change, as it has been proposed for analysing tide gauge data (e.g. Mitrovica et al., 2018). However this requires that other effects can be either corrected for (e.g. relying on models for glacial isostatic adjustment), or are small when compared to the signal of interest. While for validating large-scale mass redistribution at least over Europe this will hardly be the case, this idea could be explored for clocks that are brought deliberately close to large mass redistributions such as e.g. glaciers. Finally, since several subsidence processes evolve nearly linear in time one could simply rely on de-trending clock comparison time series; again the downside would be that most of the climate signal would be lost, unfortunately.

Assuming that optical clocks would reach an uncertainty limit corresponding to scenario 2, i.e. 10^{-19} , within a few years from now, while at the same time becoming more affordable and easier to operate, a denser and more widespread network could be pictured (see Fig. 12). Increasing the number of clocks instead of their precision and accuracy might be a more desirable objective, mainly for the following reasons. First, when GNSS becomes a limiting factor for clock comparisons, it will just not be beneficial to use better clocks. Moreover, while GRACE/-FO and possibly future satellite gravity missions will inevitably be limited in resolving a high spatial resolution (e.g. Pail et al., 2015; Flechtner et al., 2016; Rodell et al., 2018), a sufficiently dense clock network could fill this gap. In order to demonstrate the potential benefit of this strategy, Fig. 12 visualizes geoid height changes caused by the atmospheric mass redistribution in June 2007 with respect to the 2007 mean. While in panel a) one can see the full signal, in b) the geoid-height anomalies are only shown point-wise, at the clock locations of our simulated network (compare Fig. 1). In Fig. 12c) we assume a denser network; geoid-height changes are here shown at all EUREF Permanent

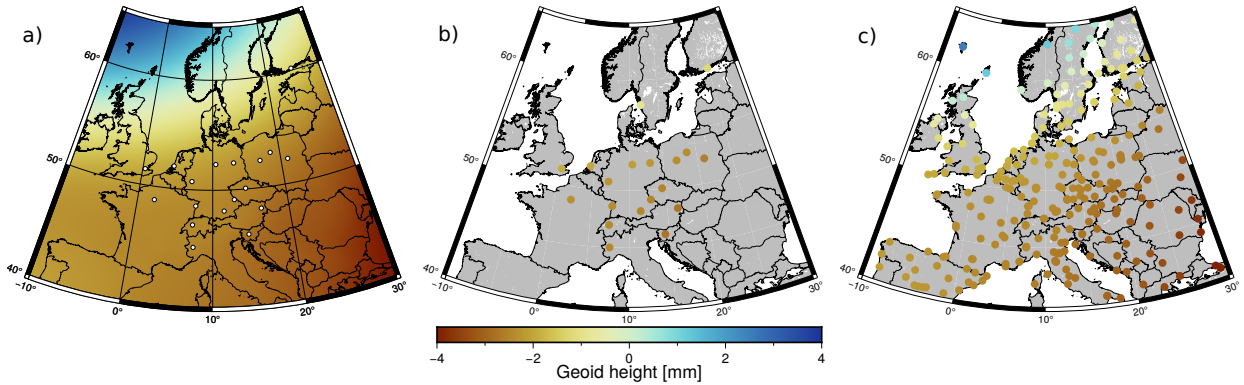


Figure 12. Visualization of geoid height anomalies in June 2007 with respect to the 2007 mean. a) visualizes the full signal, b) shows point-wise anomalies at the clock locations in our assumed network from Fig. 1, and in c) the anomalies are shown at the locations of all EUREF Permanent Network (EPN) GNSS stations. Network (EPN) GNSS stations (Bruyninx et al., 2019). The shorter distances between the almost 300 station locations would allow for gravity potential estimation with a spatial resolution even beyond what multi-pair satellite gravity missions are expected to provide (Elsaka et al., 2014).

We confront the expected spatial scale and magnitude of time-variable gravity signals against the uncertainty of clock network comparisons with associated GNSS height control within the three scenarios that we considered (see Table 1) in Fig. 13, for two different temporal scales similar to Pail et al. (2015). The GRACE uncertainty (a) here is taken from Pail et al. (2015). The network resolution limits are derived here from Fig. 1, where the longest distance (Helsinki - Torino) is about 2000 km. We have assumed four links (Warsaw - Torun, Torun - Posen, Munich - Wettzell,

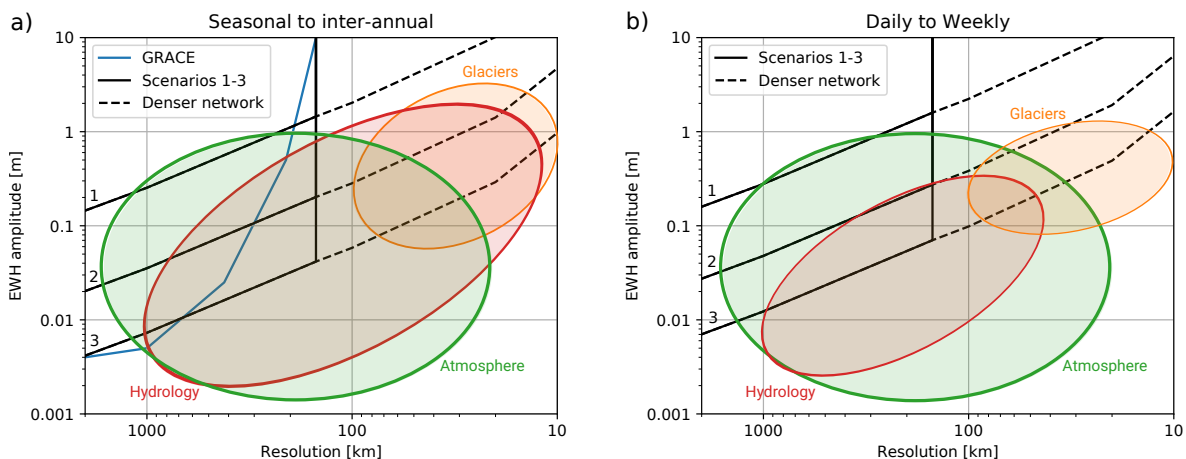


Figure 13. Magnitude versus spatial scale of the here discussed mass redistribution signals for two different temporal scales.

Braunschweig - Potsdam) slightly below 200 km distance, where we set the lower bound for the clock network resolution in the plot. Dashed lines would visualize the detectability of mass changes by a densified network as suggested in this Section. We assume that the spatial resolution has no effect on the uncertainty of geoid height changes measured by the clock network, since we assume the length of the fibre links to be irrelevant. We note that in Fig. 13 the network's uncertainty in detecting EWH changes increases with increasing resolution, however the reason for that is merely that mass redistributions at smaller scales have smaller influence on the geoid (compare Eq. 3-5). GRACE, however, exhibits a steeper increase of uncertainty with increasing resolution, mainly due to a higher signal-to-noise ratio resulting from its altitude. Thus, it becomes clear that an optical clock network would observe contributions of hydrologic and atmospheric mass changes which are likely not visible in current GRACE/-FO data, and which would possibly also not be visible in data obtained from future gravity missions. At daily to weekly scales (Fig. 13b), we do not show the GRACE curve as the standard release of GRACE products is of monthly resolution. This may change with future gravity missions though, at least for larger spatial scales and depending on their configuration and instrumentation. On the other hand, Fig. 13b) reveals that – at least over Europe – the densification of the clock network of scenario 1 would not be beneficial, because no loading signals on the smaller scales are strong enough to be detected.

Fig. 14 shows a comparison of the simulated clock links Bern - Braunschweig (left) and Bonn - Braunschweig (right) vs. simulated GRACE measurements, where the simulated signal is generated here only by the atmospheric variability. The transparent blue areas display the error bounds of the clock comparison under the three scenarios, while scenario 1 leads to error bounds beyond the axis limits here. In contrast to that, we demonstrate GRACE error bounds resulting from the error propagation of ITSG-2018 formal errors. We have decided against applying a filter because it corrupts the comparability of the GRACE errors and the point-wise clock errors. This is due to the fact that the GRACE errors refer to an area around a point instead of a point; the size of the area depends on the maximum spherical harmonic degree, while for point errors one would need infinitely many SHC's. Instead we truncated the spherical harmonic coefficients at different degrees. Truncating the SHC's at degree 60 leads to error bounds at roughly the same extension as

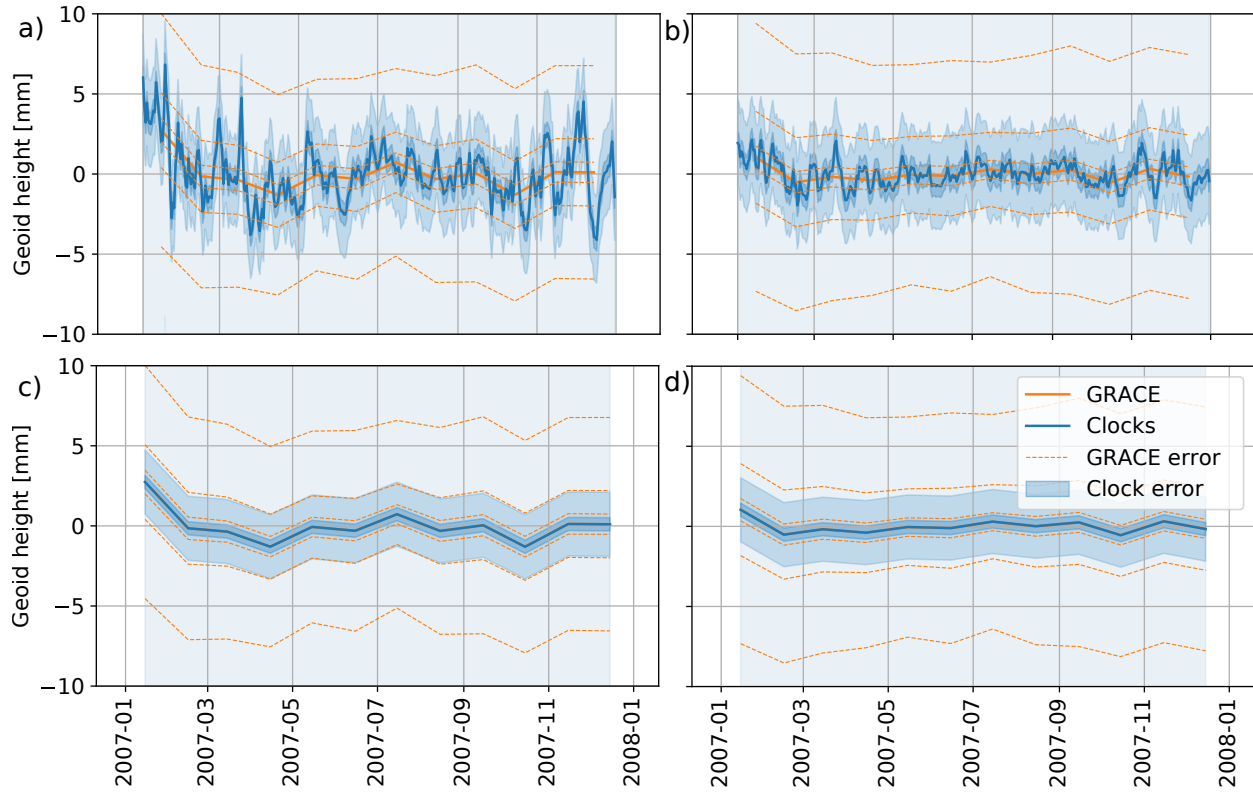


Figure 14. Time series of atmosphere induced geoid height variations of **Bern vs. Braunschweig** in the first column and **Bonn vs. Braunschweig** in the second column. Comparison of the time series as would be seen from clock comparisons and simulated GRACE data. In the second row, the daily clock measurements are averaged to a monthly resolution. 1σ error bounds are added, for the three different clock network error scenarios in transparent blue, and for the GRACE errors with dashed orange lines. The GRACE errors are ITSG-2018 formal errors, truncated at degrees 60 (smallest error bounds), 80, and 100 (largest error bounds), propagated to the geoid height difference between the two locations.

the error bounds from the clock scenario 3, i.e. with 10^{-20} clock uncertainty and 0.3 mm GNSS uncertainty. This can be observed more distinctly when the clock comparison time series is averaged to a GRACE-like monthly resolution. If the maximum spherical harmonic degree of the GRACE formal errors is increased to 80, the error bounds increase as well and are in the same range as the error bounds from clock scenario 2, i.e. with 10^{-19} clock uncertainty and 0.7 mm GNSS uncertainty. We suggest that a time series comparison between a clock comparison and satellite gravimetry observations would have to be conducted applying different truncation degrees and possibly by correcting clock readings with local or regional model data.

It has been proposed that terrestrial water storage anomalies (TWSA), as an Essential Climate

Variable (ECV), would be monitored from space at least with spatial resolution of 300 km at monthly timescale, and with a measurement accuracy of 10-20 mm monthly and 10 mm yr⁻¹ for trends. Assuming that this spatial resolution may be met by a clock network, this translates into an uncertainty of 0.1 to 0.2 mm necessary for the network's overall geoid height estimation, so slightly below our assumed scenario 3.

In order to validate – over Europe – a future gravity mission that we assume is about as precise as GRACE, a clock network would require a comparison error not greater than 2 mm geoid height, including link performance and GNSS control. This would work mostly for spatial scales of 200 to 400 km, while beyond that the GRACE precision exceeds the limits of the proposed clock network. Assuming that the future gravity mission is about five times as precise as compared to GRACE, the same clock network could be used for validation at 200 to 300 km spatial resolution of the gravity mission data.

6 SUMMARY AND CONCLUSIONS

In this work, we have simulated the effects of mass redistribution within the atmosphere, terrestrial water storage, and glaciers over Europe and the resulting geopotential change on optical clock comparisons in a possible future clock network, which would be connected with colocated GNSS receivers. We went beyond previous investigations of these effects (Voigt et al., 2016), and constructed three error scenarios for such a network, that also account for GNSS height control, in order to analyse which effects would be observable against the noise level. Hydrologic signals such as groundwater storage changes are comparably small over Europe and thus would hardly be seen under the most pessimistic scenario 1, i.e. when noise levels correspond to 10^{-18} . At monthly and longer timescales however, they could be observed under scenarios 2 and 3, i.e. assuming uncertainties of 10^{-19} and 10^{-20} , respectively, can be met for clocks and uncertainties of less than a millimeter for GNSS. As expected, we find that the influence of atmospheric mass variability is larger than for hydrological mass variability, with weekly and longer frequencies being detectable even under scenario 1, while in scenario 2 and 3 clock comparisons via a fibre network without loss of accuracy would enable one to observe even most of the daily signal. In contrast we find that glacier mass change in the European Alps and in the Scandinavian mountains would not contribute significantly to the clocks' observed signal. However, we note that in our scenarios clocks were assumed to be operated at existing national metrology laboratories and were not assumed to be transported and operated at designated observatories close to glaciers.

The GRACE and GRACE-FO missions observe in principle the same potential variations, due mass redistribution within the same compartments of the Earth system as considered here; apart from the direct effect of vertical land motion on potential, which we here suggest would have to be corrected for, using vertical height change measurements from colocated GNSS. At this point we can conclude that a network of optical clocks could provide a new tool for GRACE validation. However, GNSS uncertainty would inevitably place limits on solving the geopotential change from time-differencing clock comparisons over long distances; clock comparisons with an uncertainty of 10^{-20} fractional frequency difference do not yield a significant gain compared to comparisons at 10^{-19} , if a relative vertical motion of the clocks cannot be monitored beyond the 1 mm limit. Still,

even if vertical height control is going to be a limiting factor for clock comparisons, the number of clocks can still be increased, which would benefit the network in particular in detecting variations of smaller spatial scale.

We have not included non-tidal ocean loading in our simulations since most stations of our hypothetical network are located inland and for observing sea level changes and ocean loading, we argue that one would rather devise a network along coastal sites e.g. colocated with tide gauges. Furthermore, here we only looked at daily and longer variations. But, unless clock readings can be averaged over the whole day, tidal and nontidal subdaily variations would need to be considered by applying correction models due to aliasing effects.

In this contribution we have assumed that time-differencing clock comparisons in a regional network would be analysed with respect to the GRACE data similar to how the superconducting gravimeter community works: Time-series of spectrally limited GRACE mass change are directly compared at instrument locations to measured time series which are to be corrected for local effects. We hypothesize that this correction is much easier to derive for clock measurements since they refer to the geoid while gravimeters refer to gravity, but one could nevertheless resort to common-mode isolation techniques such as Empirical Orthogonal Function analysis (EOF, Crossley et al., 2012; van Camp et al., 2014). Eventually, local effect such as groundwater table variations, snow depth or barometric pressure changes would have to be monitored.

We conclude that in order to validate a future gravity mission that is about five times as precise as GRACE at monthly resolution, a clock network with a comparison error of maximally 2 mm geoid height would be needed, i.e. roughly our assumed scenario 2. It could be used for validation of the higher spatial scales of the gravity mission, i.e. 200 to 300 km. For the monitoring of terrestrial water storage anomalies as an essential climate variable, proposed to be measured with 10 to 20 mm accuracy at 300 km spatial resolution, the clock network error level would need to be at the level of our assumed scenario 3, i.e. below 0.5 mm geoid height. At daily to weekly scales, the network of fibre-connected clocks that we consider here could additionally observe atmospheric mass changes under scenarios 2 and 3, and it could resolve hydrological mass changes

in Europe under scenario 3, thus adding to the water cycle monitoring of a satellite gravity mission at daily temporal resolution.

ACKNOWLEDGMENTS

The research leading to these results has received funding from the European Union's Horizon 2020 research and innovation programme under Grant Agreement No. 951886 (CLONETS-DS). We acknowledge partial support by the German Science Foundation DFG via the Research Unit NEROGRAV (KU1207/29-1). Furthermore, we would like to thank Anne Springer and Anna Klos for helpful and interesting discussions.

DATA AVAILABILITY

All data used in this work can be received from the authors upon reasonable request.

References

- Agnew, D. C. & Larson, K. M., 2007. Finding the repeat times of the GPS constellation, *GPS Solut.*, **11**(1), 71–76, doi:10.1007/s10291-006-0038-4.
- Bos, M. S., Fernandes, R. M. S., Williams, S. D. P., & Bastos, L., 2013. Fast error analysis of continuous GNSS observations with missing data, *J. Geod.*, **87**(4), 351–360, doi:10.1007/s00190-012-0605-0.
- Bothwell, T., Kedar, D., Oelker, E., Robinson, J. M., Bromley, S. L., Tew, W. L., Ye, J., & Kennedy, C. J., 2019. JILA SrI optical lattice clock with uncertainty of 2.0×10^{-18} , *Metrologia*, **56**(6), 065004, doi:10.1088/1681-7575/ab4089.
- Bruyninx, C., Legrand, J., Fabian, A., & Pottiaux, E., 2019. GNSS metadata and data validation in the EUREF Permanent Network, *GPS Solut.*, **23**(4), 106, doi:10.1007/s10291-019-0880-9.
- Chanard, K., Fleitout, L., Calais, E., Reischung, P., & Avouac, J.-P., 2018. Toward a Global Horizontal and Vertical Elastic Load Deformation Model Derived from GRACE

- and GNSS Station Position Time Series, *J. Geophys. Res. Solid Earth*, **123**(4), 3225–3237, doi:10.1002/2017JB015245.
- Cheng, M. & Ries, J., 2017. The unexpected signal in GRACE estimates of C_{20} , *J. Geod.*, **91**(8), 897–914, doi:10.1007/s00190-016-0995-5.
- Chiodo, N., Quintin, N., Stefani, F., Wiotte, F., Camisard, E., Chardonnet, C., Santarelli, G., Amy-Klein, A., Pottie, P.-E., & Lopez, O., 2015. Cascaded optical fiber link using the internet network for remote clocks comparison, *Opt. Express, OE*, **23**(26), 33927–33937, doi:10.1364/OE.23.033927.
- Chou, C. W., Hume, D. B., Rosenband, T., & Wineland, D. J., 2010. Optical Clocks and Relativity, *Science*, **329**(5999), 1630–1633, doi:10.1126/science.1192720.
- Copernicus Climate Change Service (C3S), 2017. ERA5: Fifth generation of ECMWF atmospheric reanalyses of the global climate, Copernicus Climate Change Service Climate Data Store (CDS). Accessed: 28-10-2020. <https://cds.climate.copernicus.eu/cdsapp>.
- Crossley, D., Linage, C. d., Hinderer, J., Boy, J.-P., & Famiglietti, J., 2012. A comparison of the gravity field over Central Europe from superconducting gravimeters, GRACE and global hydrological models, using EOF analysis, *Geophys. J. Int.*, **189**(2), 877–897, doi:10.1111/j.1365-246X.2012.05404.x.
- Crossley, D. J., Boy, J.-P., Hinderer, J., Jahr, T., Weise, A., Wziontek, H., Abe, M., & Förste, C., 2014. Comment on: ‘The quest for a consistent signal in ground and GRACE gravity time-series’, by Michel Van Camp, Olivier de Viron, Laurent Metivier, Bruno Meurers and Olivier Francis, *Geophys. J. Int.*, **199**(3), 1811–1817, doi:10.1093/gji/ggu259.
- Davis, J. L., Elósegui, P., Mitrovica, J. X., & Tamisiea, M. E., 2004. Climate-driven deformation of the solid Earth from GRACE and GPS, *Geophys. Res. Lett.*, **31**(24), doi:10.1029/2004GL021435.
- Dobslaw, H., Bergmann-Wolf, I., Forootan, E., Dahle, C., Mayer-Gürr, T., Kusche, J., & Flechtner, F., 2016. Modeling of present-day atmosphere and ocean non-tidal de-aliasing errors for future gravity mission simulations, *J. Geod.*, **90**(5), 423–436, doi:10.1007/s00190-015-0884-3.
- Elsaka, B., Raimondo, J.-C., Brieden, P., Reubelt, T., Kusche, J., Flechtner, F., Iran Pour, S.,

- Sneeuw, N., & Müller, J., 2014. Comparing seven candidate mission configurations for temporal gravity field retrieval through full-scale numerical simulation, *J. Geod.*, **88**(1), 31–43, doi:10.1007/s00190-013-0665-9.
- Flechtner, F., Neumayer, K.-H., Dahle, C., Dobsław, H., Fagiolini, E., Raimondo, J.-C., & Güntner, A., 2016. What Can be Expected from the GRACE-FO Laser Ranging Interferometer for Earth Science Applications?, *Surv. Geophys.*, **37**(2), 453–470, doi:10.1007/s10712-015-9338-y.
- Forootan, E., Didova, O., Kusche, J., & Löcher, A., 2013. Comparisons of atmospheric data and reduction methods for the analysis of satellite gravimetry observations, *J. Geophys. Res. Solid Earth*, **118**(5), 2382–2396, doi:10.1002/jgrb.50160.
- Giorgi, G., Schmidt, T. D., Trainotti, C., Mata-Calvo, R., Fuchs, C., Hoque, M. M., Berdermann, J., Furthner, J., Günther, C., Schuldt, T., Sanjuan, J., Gohlke, M., Oswald, M., Braxmaier, C., Balidakis, K., Dick, G., Flechtner, F., Ge, M., Glaser, S., König, R., Michalak, G., Murböck, M., Semmling, M., & Schuh, H., 2019. Advanced technologies for satellite navigation and geodesy, *Adv. Space Res.*, **64**(6), 1256–1273, doi:10.1016/j.asr.2019.06.010.
- Glaser, S., Michalak, G., Männel, B., König, R., Neumayer, K.-H., & Schuh, H., 2020. Reference system origin and scale realization within the future GNSS constellation "Kepler" (accepted), *J. Geod.*.
- Grebing, C., Al-Masoudi, A., Dörscher, S., Häfner, S., Gerginov, V., Weyers, S., Lipphardt, B., Riehle, F., Sterr, U., & Lisdat, C., 2016. Realization of a timescale with an accurate optical lattice clock, *Optica*, **3**(6), 563–569, doi:10.1364/OPTICA.3.000563.
- Gruszczynska, M., Rosat, S., Klos, A., Gruszczynski, M., & Bogusz, J., 2018. Multichannel Singular Spectrum Analysis in the Estimates of Common Environmental Effects Affecting GPS Observations, *Pure Appl. Geophys.*, **175**(5), 1805–1822, doi:10.1007/s00024-018-1814-0.
- Harris, I., Jones, P. D., Osborn, T. J., & Lister, D. H., 2014. Updated high-resolution grids of monthly climatic observations – the CRU TS3.10 Dataset, *Int. J. Climatol.*, **34**(3), 623–642, doi:10.1002/joc.3711.
- Hofmann-Wellenhof, B. & Moritz, H., 2005. *Physical geodesy*, SpringerWienNewYork, Wien ; New York, 1st edn.

- Klos, A., Bogusz, J., Figurski, M., & Gruszczynski, M., 2016. Error analysis for European IGS stations, *Stud Geophys Geod*, **60**(1), 17–34, doi:10.1007/s11200-015-0828-7.
- Klos, A., Olivares, G., Teferle, F. N., Hunegnaw, A., & Bogusz, J., 2017. On the combined effect of periodic signals and colored noise on velocity uncertainties, *GPS Solut.*, **22**(1), 1, doi:10.1007/s10291-017-0674-x.
- Koller, S., Grotti, J., Vogt, S., Al-Masoudi, A., Dörscher, S., Häfner, S., Sterr, U., & Lisdat, C., 2017. Transportable Optical Lattice Clock with 7×10^{-17} Uncertainty, *Phys. Rev. Lett.*, **118**(7), 073601, doi:10.1103/PhysRevLett.118.073601.
- Krehlik, P., Śliwaczyński, L., Dostal, J., Radil, J., Smotlacha, V., Velc, R., Vojtěch, J., Campanella, M., Calonico, D., Clivati, C., Levi, F., Číp, O., Rerucha, S., Holzwarth, o., Lessing, M., Camargo, F., Desruelle, B., Lautier-Gaud, J., English, E. L., Kronjäger, J., Whibberley, P., Pottie, P., Tavares, R., Tuckey, P., John, F., Šnajder, M., Štef, J., Nogaś, P., Urbaniak, R., Binczewski, A., Bogacki, W., Turza, K., Grosche, G., Schnatz, H., Camisard, E., Quintin, N., Diaz, J., Ros, E., Galardini, A., Seeds, A., Zhen Yang, & Amy-Klein, A., 2017. CLONETS - clock network services: Strategy and innovation for clock services over optical-fibre networks, *19th International Conference on Transparent Optical Networks (ICTON), Girona, 2017*, pp. 1–2, doi:10.1109/ICTON.2017.8024939.
- Leßmann, L. & Müller, J., 2018. Analysis of non-tidal ocean loading for gravitational potential observations in northern Europe, *J. Geodyn.*, **119**, 23–28, doi:10.1016/j.jog.2018.05.008.
- Lion, G., Panet, I., Wolf, P., Guerlin, C., Bize, S., & Delva, P., 2017. Determination of a high spatial resolution geopotential model using atomic clock comparisons, *J. Geod.*, **91**(6), 597–611, doi:10.1007/s00190-016-0986-6.
- Lisdat, C., Grosche, G., Quintin, N., Shi, C., Raupach, S. M. F., Grebing, C., Nicolodi, D., Stefani, F., Al-Masoudi, A., Dörscher, S., Häfner, S., Robyr, J.-L., Chiodo, N., Bilicki, S., Bookjans, E., Koczwara, A., Koke, S., Kuhl, A., Wiotte, F., Meynadier, F., Camisard, E., Abgrall, M., Lours, M., Legero, T., Schnatz, H., Sterr, U., Denker, H., Chardonnet, C., Coq, Y. L., Santarelli, G., Amy-Klein, A., Targat, R. L., Lodewyck, J., Lopez, O., & Pottie, P.-E., 2016. A clock network for geodesy and fundamental science, *Nat Commun*, **7**(1), 1–7, doi:10.1038/ncomms12443.

- Ludlow, A. D., Boyd, M. M., Ye, J., Peik, E., & Schmidt, P., 2015. Optical atomic clocks, *Rev. Mod. Phys.*, **87**(2), 637–701, doi:10.1103/RevModPhys.87.637.
- Maussion, F., Butenko, A., Champollion, N., Dusch, M., Eis, J., Fourteau, K., Gregor, P., Jarosch, A. H., Landmann, J., Oesterle, F., Recinos, B., Rothenpieler, T., Vlug, A., Wild, C. T., & Marzeion, B., 2019. The Open Global Glacier Model (OGGM) v1.1, *Geosci. Model Dev.*, **12**(3), 909–931, doi:10.5194/gmd-12-909-2019.
- Mayer-Gürr, T., Behzadpur, S., Ellmer, M., Kvas, A., Klinger, B., Strasser, S., & Zehentner, N., 2018. ITSG-Grace2018 - Monthly, Daily and Static Gravity Field Solutions from GRACE, GFZ Data Services. doi:10.5880/ICGEM.2018.003.
- Mehlstäubler, T., Grosche, G., Lisdat, C., Schmidt, P., & Denker, H., 2018. Atomic Clocks for Geodesy, *Rep. Prog. Phys.*, **81**(6), 064401, doi:10.1088/1361-6633/aab409.
- Mitrovica, J. X., Hay, C. C., Kopp, R. E., Harig, C., & Latychev, K., 2018. Quantifying the Sensitivity of Sea Level Change in Coastal Localities to the Geometry of Polar Ice Mass Flux, *J. Climate*, **31**(9), 3701–3709, doi:10.1175/JCLI-D-17-0465.1.
- Oelker, E., Hutson, R. B., Kennedy, C. J., Sonderhouse, L., Bothwell, T., Goban, A., Kedar, D., Sanner, C., Robinson, J. M., Marti, G. E., Matei, D. G., Legero, T., Giunta, M., Holzwarth, R., Riehle, F., Sterr, U., & Ye, J., 2019. Demonstration of 4.8×10^{-17} stability at 1 s for two independent optical clocks, *Nat. Photonics*, **13**(10), 714–719, doi:10.1038/s41566-019-0493-4.
- Oleson, K. W., Bonan, G. B., Schaaf, C., Gao, F., Jin, Y., & Strahler, A., 2003. Assessment of global climate model land surface albedo using MODIS data, *Geophys. Res. Lett.*, **30**(8), doi:10.1029/2002GL016749.
- Pail, R., Bingham, R., Braitenberg, C., Dobslaw, H., Eicker, A., Güntner, A., Horwath, M., Ivins, E., Longuevergne, L., Panet, I., Wouters, B., & IUGG Expert Panel, 2015. Science and User Needs for Observing Global Mass Transport to Understand Global Change and to Benefit Society, *Surv. Geophys.*, **36**(6), 743–772, doi:10.1007/s10712-015-9348-9.
- Panet, I., Flury, J., Biancale, R., Gruber, T., Johannessen, J., van den Broeke, M. R., van Dam, T., Gegout, P., Hughes, C. W., Ramillien, G., Sasgen, I., Seoane, L., & Thomas, M., 2013. Earth System Mass Transport Mission (e.motion): A Concept for Future Earth Gravity Field

- Measurements from Space, *Surv. Geophys.*, **34**(2), 141–163, doi:10.1007/s10712-012-9209-8.
- Poli, N., Oates, C. W., Gill, P., & Tino, G. M., 2013. Optical atomic clocks, *Riv. del Nuovo Cim.*, **36**(12), 555–624, doi:10.1393/ncr/i2013-10095-x.
- Raupach, S. M. F., Koczwara, A., & Grosche, G., 2015. Brillouin amplification supports 1×10^{-20} uncertainty in optical frequency transfer over 1400 km of underground fiber, *Phys. Rev. A*, **92**(2), 021801, doi:10.1103/PhysRevA.92.021801.
- Riley, W. & Howe, D. A., 2008. Handbook of Frequency Stability Analysis | NIST, *Special Publication (NIST SP) - 1065*, <https://www.nist.gov/publications/handbook-frequency-stability-analysis>.
- Rodell, M., Famiglietti, J. S., Wiese, D. N., Reager, J. T., Beaudoin, H. K., Landerer, F. W., & Lo, M.-H., 2018. Emerging trends in global freshwater availability, *Nature*, **557**(7707), 651–659, doi:10.1038/s41586-018-0123-1.
- Schioppo, M., Brown, R. C., McGrew, W. F., Hinkley, N., Fasano, R. J., Beloy, K., Yoon, T. H., Milani, G., Nicolodi, D., Sherman, J. A., Phillips, N. B., Oates, C. W., & Ludlow, A. D., 2017. Ultrastable optical clock with two cold-atom ensembles, *Nat. Photonics*, **11**(1), 48–52, doi:10.1038/nphoton.2016.231.
- Schumacher, M., Kusche, J., & Döll, P., 2016. A systematic impact assessment of GRACE error correlation on data assimilation in hydrological models, *J. Geod.*, **90**(6), 537–559, doi:10.1007/s00190-016-0892-y.
- Skamarock, C., Klemp, B., Dudhia, J., Gill, O., Barker, D., Duda, G., Huang, X.-y., Wang, W., & Powers, G., 2008. A Description of the Advanced Research WRF Version 3, University Corporation for Atmospheric Research. doi:10.5065/D68S4MVH.
- Takamoto, M., Ushijima, I., Ohmae, N., Yahagi, T., Kokado, K., Shinkai, H., & Katori, H., 2020. Test of general relativity by a pair of transportable optical lattice clocks, *Nat. Photonics*, **14**, 411–415, doi:10.1038/s41566-020-0619-8.
- Takano, T., Takamoto, M., Ushijima, I., Ohmae, N., Akatsuka, T., Yamaguchi, A., Kuroishi, Y., Munekane, H., Miyahara, B., & Katori, H., 2016. Geopotential measurements with synchronously linked optical lattice clocks, *Nat. Photonics*, **10**(10), 662–666,

doi:10.1038/nphoton.2016.159.

- Tapley, B. D., Watkins, M. M., Flechtner, F., Reigber, C., Bettadpur, S., Rodell, M., Sasgen, I., Famiglietti, J. S., Landerer, F. W., Chambers, D. P., Reager, J. T., Gardner, A. S., Save, H., Ivins, E. R., Swenson, S. C., Boening, C., Dahle, C., Wiese, D. N., Dobslaw, H., Tamisiea, M. E., & Velicogna, I., 2019. Contributions of GRACE to understanding climate change, *Nat. Clim. Chang.*, **9**(5), 358–369, doi:10.1038/s41558-019-0456-2.
- Turza, K., Krehlik, P., & Śliwczyński, L., 2020. Stability Limitations of Optical Frequency Transfer in Telecommunication DWDM Networks, *IEEE Trans. Ultrason. Ferroelectr. Freq. Control*, **67**(5), 1066–1073, doi:10.1109/TUFFC.2019.2957176.
- van Camp, M., Viron, O. d., Métivier, L., Meurers, B., & Francis, O., 2014. The quest for a consistent signal in ground and GRACE gravity time-series, *Geophys. J. Int.*, **197**(1), 192–201, doi:10.1093/gji/ggt524.
- Villiger, A. & Dach, R., 2020. International GNSS Service: Technical Report 2019, Technical report, IGS Central Bureau and University of Bern Open Publishing, doi:10.7892/boris.144003.
- Voigt, C., Denker, H., & Timmen, L., 2016. Time-variable gravity potential components for optical clock comparisons and the definition of international time scales, *Metrologia*, **53**, 1365, doi:10.1088/0026-1394/53/6/1365.
- Wahr, J., Molenaar, M., & Bryan, F., 1998. Time variability of the Earth's gravity field: Hydrological and oceanic effects and their possible detection using GRACE, *J. Geophys. Res. Solid Earth*, **103**(B12), 30205–30229, doi:10.1029/98JB02844.
- WCRP Global Sea Level Budget Group, 2018. Global sea-level budget 1993–present, *Earth Syst. Sci. Data*, **10**(3), 1551–1590, doi:10.5194/essd-10-1551-2018.
- Williams, S. D. P., Bock, Y., Fang, P., Jamason, P., Nikolaidis, R. M., Prawirodirdjo, L., Miller, M., & Johnson, D. J., 2004. Error analysis of continuous GPS position time series, *J. Geophys. Res. Solid Earth*, **109**(B3), doi:10.1029/2003JB002741.
- Zemp, M., Huss, M., Thibert, E., Eckert, N., McNabb, R., Huber, J., Barandun, M., Machguth, H., Nussbaumer, S. U., Gärtner-Roer, I., Thomson, L., Paul, F., Maussion, F., Kutuzov, S., & Cogley, J. G., 2019. Global glacier mass changes and their contributions to sea-level rise from

40 *Stefan Schröder et al.*

1961 to 2016, *Nature*, **568**(7752), 382–386, doi:10.1038/s41586-019-1071-0.